

Structural and magnetic properties of epitaxial Cu/Fe/Cu/Si(111) ultrathin films

G. Gubbiotti,* L. Albinì, S. Tacchi, and G. Carlotti

Istituto Nazionale per la Fisica della Materia, Dipartimento di Fisica dell'Università, Via Pascoli, I-06100 Perugia, Italy

R. Gunnella and M. De Crescenzi

Istituto Nazionale per la Fisica della Materia, Dipartimento di Matematica e Fisica dell'Università, Via Madonna delle Carceri, I-62032 Camerino, Italy

(Received 16 April 1999; revised manuscript received 14 July 1999)

Epitaxial Cu/Fe/Cu heterostructures with Fe film thicknesses between 2.5 and 110 Å were successfully grown on 7×7 -Si(111) substrates, using metal-metal epitaxy on silicon. The evolution of their structural and magnetic properties as a function of the Fe film thickness has been studied by a number of complementary techniques. This revealed that fcc pseudomorphic Fe layers, characterized by a low-spin ferromagnetic phase, grow up to about 6 Å. For larger thicknesses one observes the appearance of three-dimensional bcc Fe (110) domains in the Kurdjumov-Sachs orientation characterized by a high magnetic moment. A combined study of the magnetic anisotropy constants has been performed by the simultaneous use of both a static technique (surface magneto-optical Kerr effect) and a dynamic one (Brillouin light scattering). An excellent agreement, in both sign and magnitude, between the results of the two techniques has been found.
[S0163-1829(99)12547-5]

I. INTRODUCTION

The magnetic and structural properties of the metastable fcc phase of iron (γ -Fe) remain a controversial subject. Theoretical calculations of bulk γ -Fe predict different magnetic ground states, including a nonmagnetic state, an antiferromagnetic state, and a high- or a low-moment ferromagnetic state, with a strong dependence on the specific lattice parameter and crystal orientation.¹ Experimentally, although the face centered cubic (fcc) structure of bulk Fe is stable only in the temperature range between 1184 and 1665 K, it is possible to grow metastable ultrathin films of fcc iron at room temperature and below by epitaxially depositing Fe on Cu single crystal. Early ferromagnetic resonance investigations by Wri g^{h} ² on electrolytically prepared (110) γ -Fe films on Cu(110), as well as magnetization measurements by Gradmann *et al.*³ on (111) γ -Fe films evaporated on Cu substrates, revealed ferromagnetism at room temperature and, in the latter case, a surprisingly small magnetic moment of $0.6 \mu_B/\text{atom}$. In contrast, Mössbauer studies of epitaxial γ -Fe films prepared by vapor deposition on heated Cu(100) substrates under ultrahigh vacuum conditions, showed paramagnetism at 300 K and a transition to antiferromagnetism at lower temperatures.⁴ More recently, the occurrence of ferromagnetic coupling has been confirmed by a number of different authors who studied the Fe/Cu(100) system.⁵ Comparably few publications have been concerned with Fe grown on Cu(111).⁶ It has been reported that at room temperature Fe grows pseudomorphically up to 4 or 5 monolayers (ML) ($\cong 8\text{--}10 \text{ \AA}$) on flat Cu (111) substrate,⁷ and then transforms to bcc structure with (110) orientation.^{6,7,8} More recently Shen *et al.*⁹ carried out a similar research using a stepped Cu(111) substrate, reporting the fcc-bcc transition to take place between 2.3 and 2.7 ML ($\cong 4\text{--}6 \text{ \AA}$) of Fe. The reduced value of the critical thickness with respect to the findings

of Tian *et al.*⁷ was attributed to the different kind of substrate.

The aim of the present work is to perform a detailed analysis of the structural and magnetic properties of epitaxial γ -Fe films grown in UHV conditions on the 7×7 reconstructed (111)-Si surface, using a Cu buffer layer. Although Si does not provide a close lattice match to any of the elemental magnetic metals, we show that, when the Si(111) surface presents the characteristic 7×7 reconstruction, it may be used as seed layer upon which single crystal films of nonmagnetic metals, such as Cu, can be grown. Further epitaxial growth of metallic layers on Cu is therefore possible, achieving the so called metal-metal epitaxy on silicon (MMES), which is of potential importance for the integration of magnetic films in solid state devices. A number of complementary structural and magnetic techniques were exploited to study the deposited Fe films as a function of their thickness, in the range between 2.5 and 110 Å. Particular attention was devoted to analyze the fcc-bcc structural transition and the corresponding evolution of the magnetic properties. We show that the combined use of low-energy and Kikuchi electron diffraction yields detailed information about such phase transition providing insight into both long- and short-range order. Concerning the magnetic properties, a major result of this research is the simultaneous and combined investigation of magnetic anisotropy by use of both a static and a dynamic techniques, namely surface magneto-optical Kerr effect (SMOKE) and Brillouin light scattering (BLS). In addition, to our knowledge, no previous BLS investigations of Fe grown on Cu(111) have been reported in the literature.¹⁰

II. EXPERIMENT

Epitaxial Fe films, with thickness in the range between 2.5 and 110 Å, were prepared in a ultrahigh vacuum (UHV)

system, with a base pressure of 2×10^{-11} Torr, equipped with standard preparation and characterization facilities such as low-energy electron diffraction (LEED), Kikuchi electron diffraction (KED), and Auger electron spectroscopy (AES).¹¹ The substrate was an optically polished Si(111) crystal (*p*-type, 0.1 Ωcm) clamped on two rods for direct Joule heating. The atomic cleaning was obtained by a series of successive flashes at 1200 °C to get an *in situ* desorption of the native oxide. To reach such a temperature a current of 8 A flowing through the sample was required. This resulted in a sharp and low background reconstructed 7×7 LEED pattern whereby surface impurities including carbon and oxygen were below the Auger detection limit, which was estimated to be better than 0.5%. A 35 Å thick Cu buffer layer was used to avoid the formation of Fe silicides and/or metallic islands. In addition, a 35 Å thick Cu protective overlayer was grown on top of the Fe films to prevent from oxygen contamination during *ex situ* measurements and to have identical interfaces on both sides of the Fe film. During the evaporation of both Cu and Fe at a rate of 0.01 Å/s, the vacuum pressure rose to about 5×10^{-10} Torr. Iron deposition was made onto the Cu buffer layer flowing a current about 13 A into a Fe filament (purity 99.999%) of 1 mm in a diameter whereby the substrate temperature was kept at room temperature in order to avoid formation of copper silicides and interdiffusion between adjacent metallic layers. The film thickness was monitored by a quartz microbalance and measured *ex situ* by means of x-ray diffraction experiments in the θ - 2θ configuration.

KED measurements, which allow the investigation of the atomic structure at and below the surface of a solid were taken with the same reverse-view LEED system using an incident electron beam energy of 3 keV. KED is particularly suitable for such a kind of investigation. In fact most of the techniques which rely on electron diffraction have as a prerequisite the long range order of the arrangement of the atoms in the examined surface to render a reciprocal space image of such a surface. KED, sometimes called secondary electron imaging (SEI)¹² involves the two dimensional imaging of quasi-elastic backscattered electrons of about 1500 eV or higher. The process responsible for such an imaging of the real space structure of the surface consists in an increased ratio between inelastic/elastic scattering processes together with a dominance of the forward character of the scattering for such values of the electron kinetic energy. Consequently, the atoms of the surface act as point sources for secondary electrons which will be scattered by neighbor atoms along atomic chains aligned with the electron detector resulting in a real space projection of the real space atomic arrangement around each source. The electron coherence at these energies is fully destroyed by the Debye-Waller factor so that back-scattered electrons are mostly produced by inelastic processes. Furthermore, as the forward scattering regime is only slightly dependent on the energy an optimal contrast in the recorded image is obtained by the incoherent addition of secondary electrons with different energy (up to 100 eV of energy losses).

BLS measurements were carried out using a Sandercock-type (3+3)-pass tandem Fabry-Perot interferometer,¹³ characterized by a finesse of about 100 and a contrast ratio higher than 5×10^{10} . About 150 mW of *P*-polarized light, from an Ar⁺-ion laser operated in single longitudinal mode on the

5145-Å line, was focused onto the sample surface and the back-scattered light analyzed by the interferometer. The sample was placed between the poles of an electromagnet used to produce a dc magnetic field, with a maximum intensity of 7.0 kOe, applied parallel to the film surface and perpendicular to the plane of incidence of light. Since light scattered by magnons has its plane of polarization rotated through 90°, an analyzer was used to remove unwanted back-reflections from the objective lens and light scattered by acoustic phonons. To avoid saturation of the photon counting system, a mechanical shutter at the entrance of the interferometer interrupts the primary beam intensity during the scan across the elastic peak, while a much weaker secondary beam is used to maintain the stabilization of the interferometer.¹⁴ In the backscattering geometry, the conservation of momentum in the photon-magnon interaction implies that the spin-wave wavevector parallel to the film surface is linked to the optical wave vector k_i and to the angle of incidence θ_i by the equation $q_{\parallel} = 2k_i \sin \theta_i$. All spectra were recorded in air at room temperature at an incidence angle of light of 45° ($q_{\parallel} = 1.73 \times 10^{-5} \text{ cm}^{-1}$) with typical acquisition times of 0.5 h.

Magnetic characterization of Fe films was also performed by surface magneto-optic Kerr effect (SMOKE) using a homemade apparatus based on the differential detection method¹⁵ which increases the signal-to-noise ratio with respect to the conventional method of nearly crossed polarizers.¹⁶ Linearly polarized light from a MDL 670 laser, with wavelength of $\lambda = 6728.7 \text{ Å}$, is focused onto the sample surface. The incident light is polarized in the plane of incidence, and the reflected light goes through a $\lambda/2$ or a $\lambda/4$ wave plate and then through a Wollaston prism which spatially separates the two components of light polarization, parallel and perpendicular to the incidence plane. These intensities were detected using two SD-100-41-21-231 photodiodes from advanced Photonix. It can be demonstrated, by using the Jones matrix formalism,¹⁷ that the total Kerr signal ϕ_K , measured with the differential detection method, is either proportional to the Kerr rotation $\phi_K = 2\theta_K$, or to the Kerr ellipticity $\phi_K = 2\varepsilon_K$, depending on the use of a $\lambda/2$ or $\lambda/4$ wave plate, respectively. The hysteresis loops were recorded at room temperature both in the longitudinal and polar configuration. The maximum intensity of the external field was 400 Oe in the longitudinal configuration, and about 22 kOe in the polar one. This field was large enough to saturate the samples along the hard direction.

III. STRUCTURAL CHARACTERIZATION

The cleanliness of the Si substrate as well that of each deposited layer was controlled by AES. Figure 1(a) shows the Auger spectrum taken after the cleaning procedure of the Si substrate with $L_{2,3}VV(92 \text{ eV})$ Auger transition. No signal from contaminants like carbon or oxygen were detected within the Auger atomic sensitivity. Figures 1(b), 1(c), and 1(d) show the typical Auger spectra taken after the deposition of 35 Å of Cu, 18 Å of Fe, and again 35 Å Cu. Sizeable interdiffusion between metals and silicon can be excluded because only the characteristic Auger features of the depos-

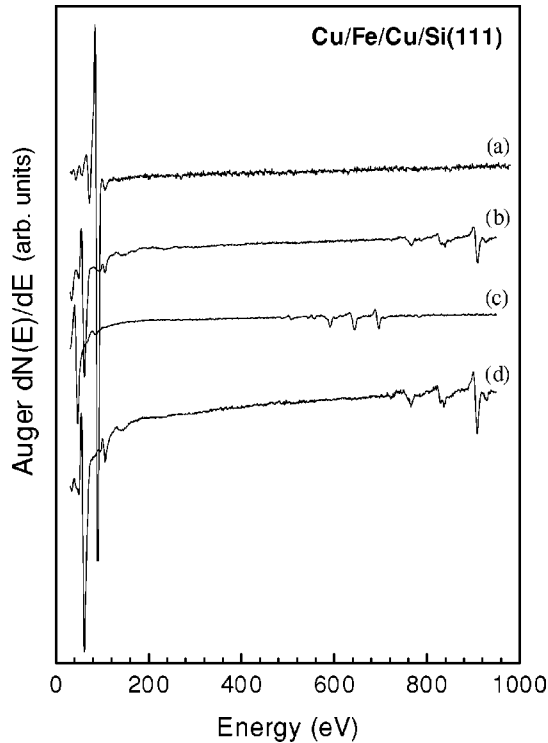


FIG. 1. Sequence of differential Auger spectra from Cu/Fe/Cu/Si(111) heterostructure. (a) Auger signal of the (111)-Si surface after the cleaning procedure described in the text, (b) Auger signal of the 35 Å thick Cu buffer layer deposited onto the Si substrate, (c) Auger signal after the deposition of 18 Å of Fe onto the Cu buffer layer (note the absence of features characteristic of Cu atoms and of alloy formation at the interface), (d) After the deposition of the 35 Å thick Cu overlayer.

ited materials have been observed. Concerning the growth of the Cu buffer layer, we have shown elsewhere using LEED and KED (Refs. 18–20) that, because of the large mismatch with Si, pseudomorphism never occurs but the Cu growth mode follows the so-called “cube on cube growth,” i.e., Cu grows with its own bulk lattice parameter and with the (111) orientation induced by the Si substrate. In particular, the Cu buffer layer consists of twinned islands producing sixfold symmetric LEED and KED patterns, unlike the threefold symmetry patterns expected for a Cu(111) single crystal.²⁰ This quite surprising result is consistent with the STM measurements made by Tosch and Neddermeyer²¹ who observed that, in the submonolayer and monolayer growth regime, the Cu layer consists of twinned bidimensional Cu islands of triangular shape, which grow mostly on top of the faulted halves of the 7×7 unit cell of Si(111) with a relative rotation of 180° .

The structural properties of the Fe layers were studied by an accurate analysis of the LEED patterns, which are reported in Fig. 2 for different energies of the primary electron beam. For Fe films 2.5 and 4 Å thick the pattern is identical to the sixfold symmetric one observed for the Cu(111) buffer layer. This corresponds to the formation of a pseudomorphic film of γ -Fe(111) favored by the low lattice mismatch between iron and copper. For fcc iron between $T = 1184$ K and

$T = 1665$ K, the nearest neighbor separation is given by $3.5832 + 7.00 \times 10^{-5} t$ Å, where t in $^\circ\text{C}$.²² Extrapolating this formula to room temperature ($t = 25^\circ\text{C}$) one obtains 3.5846 Å which is quite close to the value of the lattice parameter of Cu (3.6147 Å). Moreover, the presence of spots with equal intensity in sixfold symmetry indicates the coexistence of twinned Fe islands, with a relative rotation of 180° , induced by the Cu buffer layer.

For a Fe coverage of 6 Å or higher, the LEED pattern changes gradually, with the appearance of five satellite spots around each spot of the first pseudomorphic Fe monolayers as previously observed for Fe/Cu(111) (Ref. 7) and Fe/Ru(0001) (Ref. 23) films. This complex LEED pattern can be interpreted as due to the structural transformation of the metastable fcc Fe film in a bcc one. The new spots appearing in the LEED patterns reflect the growth of three-dimensional domains of bcc Fe(110) in the Kurdjumov-Sachs (KS) orientation^{24,25,26,27} onto the hexagonal net of pseudomorphic Fe on Cu(111). The KS orientation is a special case of the one-dimensional matching between bcc (110) and fcc (111) with sides of the rhombic unit meshes of the film parallel to those of the substrate substrate ($AB \parallel A'B'$, with a relative rotation of 5.3°). A unit mesh of the Cu(111) net is depicted in Fig. 3(a). The mesh edges are 2.556 Å long ($a_0 \times \sqrt{2}/2$ with $a_0 = 3.615$ Å) forming angles of 60° and 120° with one another. A bcc Fe(110) net is quasi-hexagonal and a suitable unit mesh is also depicted in Fig. 3(b). The mesh edges are 2.482 Å long ($a_0 \times \sqrt{3}/2$ with $a_0 = 2.866$ Å), forming angles of 70.53° and 108.47° with one another. Since there are two equivalent orientations of the direct lattice and taking into account the sixfold symmetry of the hexagonal net, it can be shown that the LEED pattern for bcc(110) domains in the KS orientation can be constructed. It consists of a cluster of six spots around the spots of the pseudomorphic Fe layer in the hexagonal symmetry (as a matter of fact only five satellite spots can be seen because two of them always merge with each other).²³ Each cluster of five spots (three inner and two outer spots) arise from the 10- and 11-type beams from Fe(110). Since beam intensities vary with electron energy, the five spots are not all clearly observable at the same energy. In our LEED patterns, the three inner spots are best observed at 90 eV for the 6 Å thick Fe film, whereas the two outer spots are well visible at 70 eV. In the case of the 12 Å thick film, the two outer spots together with a broad cluster of the three inner spots are simultaneously visible for incident beam energy of 90 eV. The satellite spots maintain the six-fold symmetry and persist up to 110 Å, the thicker Fe film studied in this work, although they undergo an appreciable broadening as the film thickness increases since the growth of rotationally related bcc Fe(110) domains introduces structural disorder in the film. A closer inspection of Fig. 2 shows that all the LEED patterns for the 6 Å thick Fe film present intense spots at the center of the five satellite spots, in a position corresponding to the hexagonal net of the underlying Fe layers pseudomorphic with Cu(111). For thicker Fe films these spots were not observed anymore in the LEED images, as the pseudomorphic fcc Fe layers were no longer reached by the electron beam.

A confirmation of the structural transformation of Fe taking place for coverage between 4 and 6 Å was also obtained

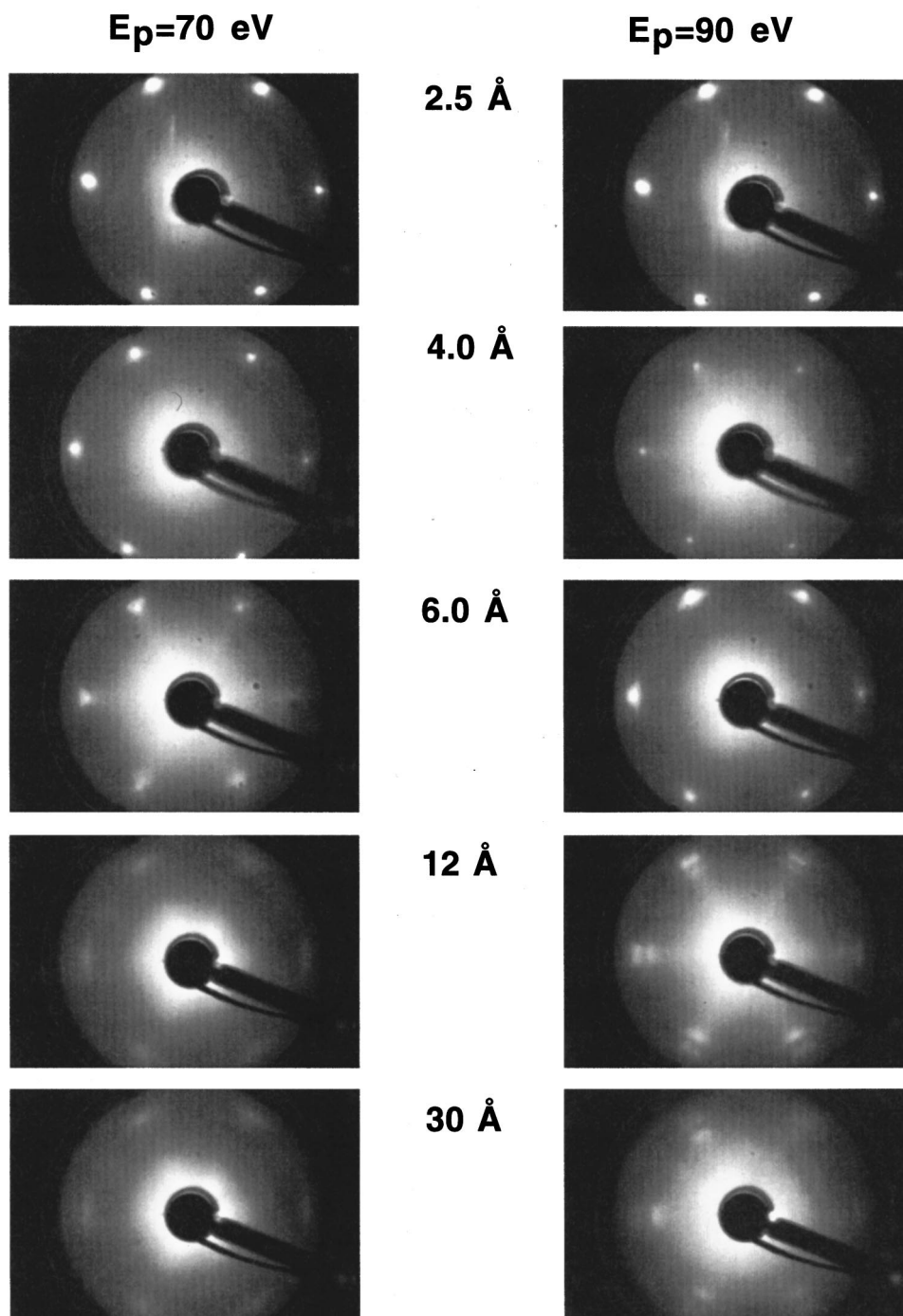


FIG. 2. LEED patterns of Fe films with different thicknesses, taken for two different energies of 70 eV (left side) and 90 eV (right side).

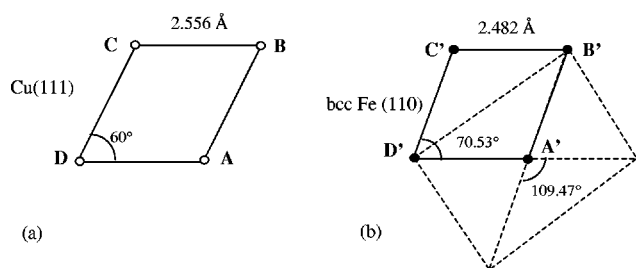


FIG. 3. (a) Unit meshes of fcc Cu(111) and (b) bcc Fe(110).

by KED investigation. Figure 4 shows KED patterns for Fe films with different thicknesses as well as for the Cu buffer and capping layers. A change in the symmetry of KED patterns when the Fe film exceeds a thickness of 6 Å is clearly visible with the appearance of spots with a sixfold symmetry, rotated by 30° with respect to those of the Cu buffer layer and to those of thinner Fe films. This type of KED symmetry, whose origin will be discussed in detail here below, persisted also when the Fe thickness was increased up to 110 Å. We note that the KED pattern of the Cu capping layer returns to be equal to that of the Cu buffer layer indicating that the

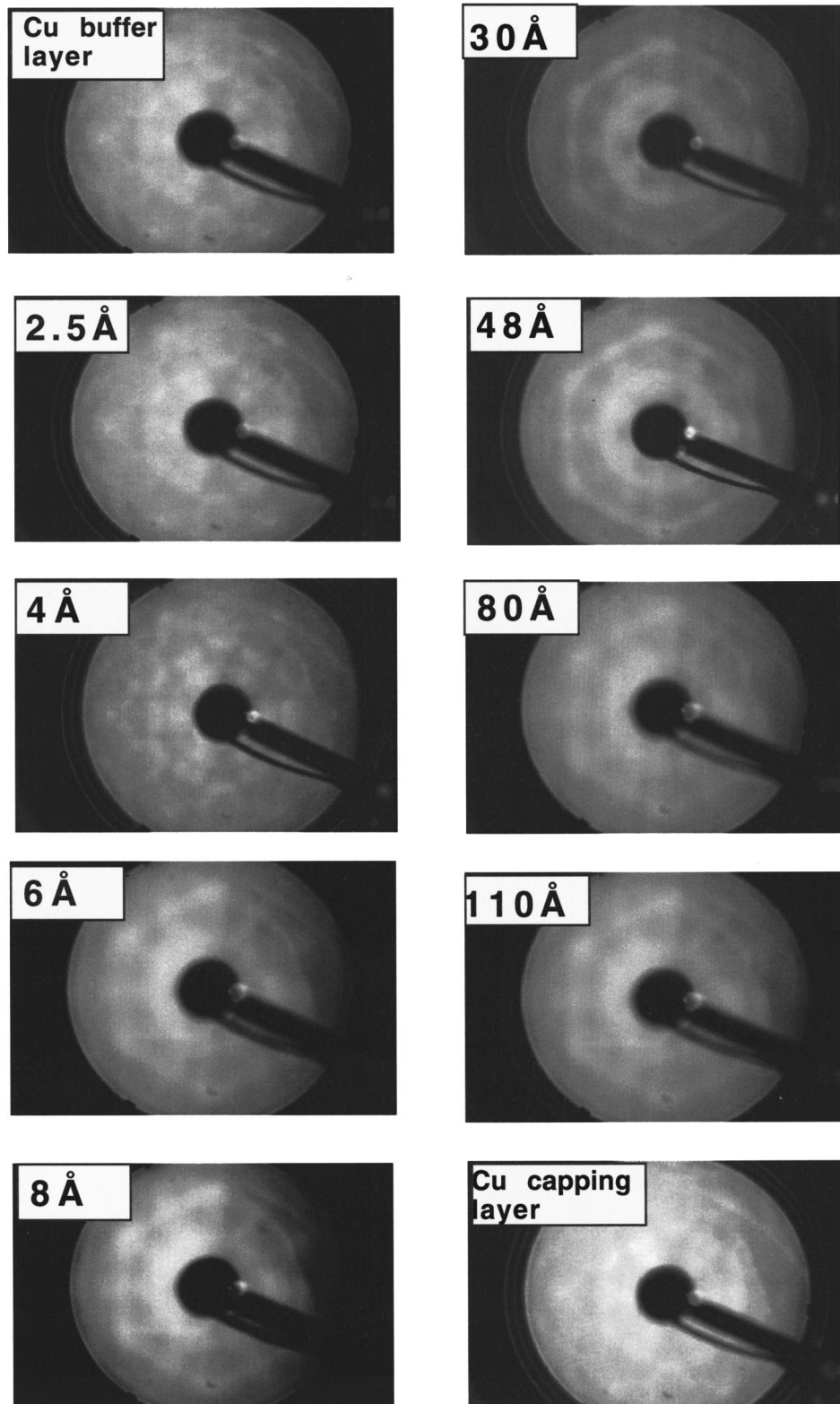


FIG. 4. Sequence of KED patterns taken at an energy 3.0 keV for the Cu(111) buffer layer, for Fe films with different thicknesses and for the Cu(111) capping layer.

modifications observed for Fe film thicker than 6 Å are due to a structural change of the Fe film itself. Different from the expected twofold symmetry of the KED pattern of a bcc(110) crystal, the observed sixfold symmetry can be explained considering the growth of bcc Fe(110) domains in the KS orientation.

To prove this assertion, we have simulated the evolution occurring in the KED images during the heteroepitaxial growth of Fe on the Cu(111) twinned surface. The calculations are performed on the basis of single scattering to describe the path of secondary electrons from the solid to the detector. A spherical correction to the electron plane wave

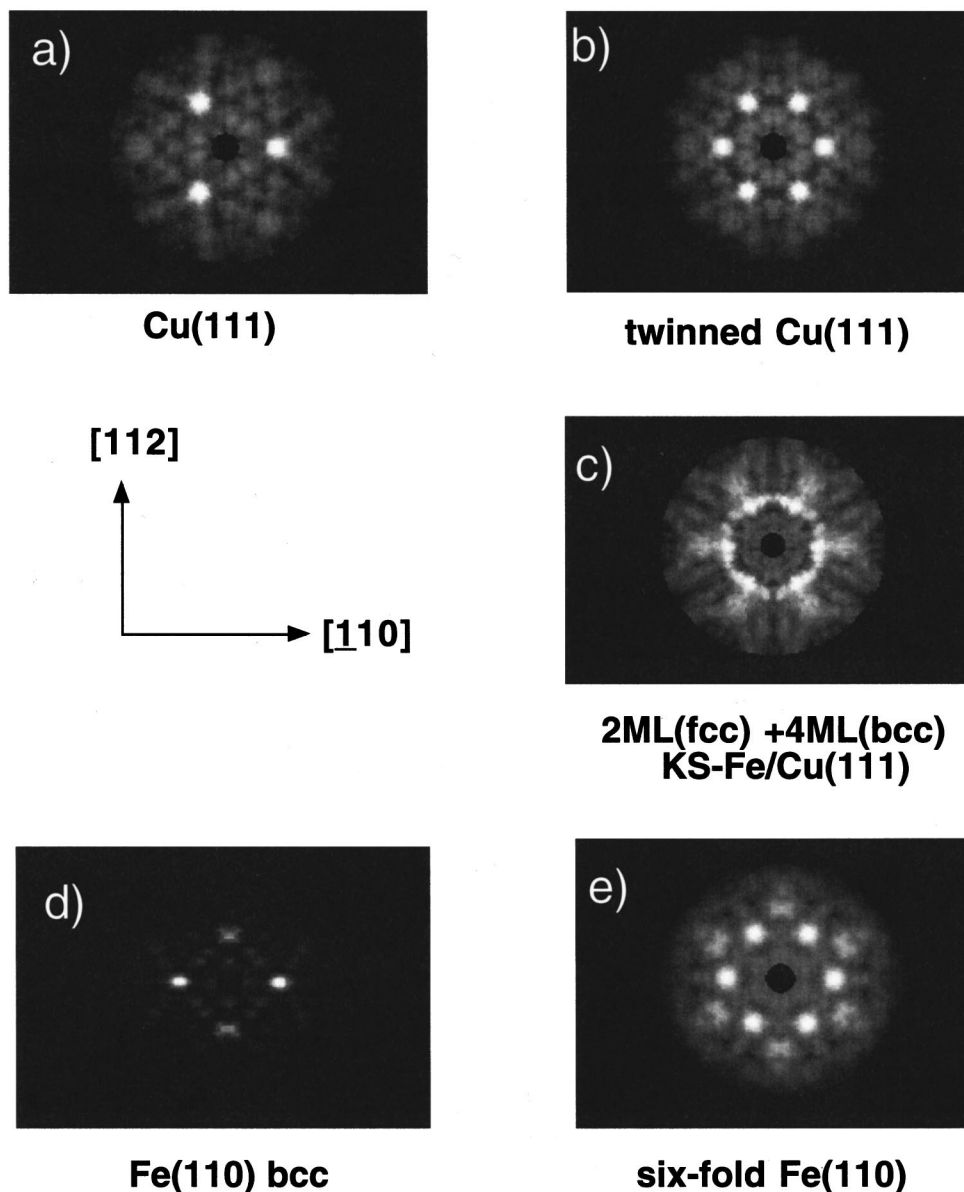


FIG. 5. (a) Simulated KED pattern of a Cu(111) surface. (b) KED pattern obtained in the case of growth with double orientation (180°) induced by the 7×7 -Si(111) surface stacking faults. (c) KED pattern obtained in the case of growth of 4 ML Fe(110) bcc + 2 ML Fe(111) fcc on twinned Cu(111) surface according to the KS orientation. (d) Fe(110) bcc KED pattern. (e) KED pattern of bcc Fe(110) arranged in sixfold symmetry.

has been used to better reproduce the electron wave front.²⁸ The model used consists in the incoherent superposition of the scattering cross section along a well defined angle of emission of all the independent sources of secondary emission excited by the 3.0 keV electron incident beam. The penetration and the escape depth has been evaluated according the well known “universal curve” proposed for the electron mean free path in solids²⁹ resulting in an estimated surface slab of about 15 atomic planes involved in the observed intensity. The evolution of the recorded projections is reported in Figs. 5(a)–5(e) as stereographic projections. In Fig. 5(a) we show the simulated Kikuchi pattern for the Cu(111) surface while the modification induced when the thin film is grown on the Si(111)- 7×7 reconstructed surface, i.e., in presence of stacking faults on such a surface which determine two different growth orientations, is shown in Fig. 5(b). At the first stage of the film deposition the contribution of fcc

Fe(111) pseudomorphic on Cu(111) would not be detectable in the KED patterns because of the similar scattering factors of the two elements and the full epitaxy of the film.

The simulated pattern which show the effect induced by 4 ML of Fe(110) bcc in KS orientation (sixfold symmetric) added to two ML of fcc-Fe(111) on Cu(111) is shown in Fig. 5(c). The close agreement with the experimental patterns observed between 6 and 8 Å is evidence of the evolution of the film structure during the transition from the fcc to bcc structure. Furthermore we note that a close resemblance between twinned (111) fcc and KS orientation on bcc is expected when the sixfold symmetry is induced during the growth. The two simulated pattern for the Fe(110) film and the effect induced by the six equivalent KS orientations on the Cu(111)/Si(111) substrate are shown in Figs. 5(d) and 5(e). We can consider that the main atomic close packed chains in the fcc (111) surface are expected at 19.5° [112], 35.4°

[011], 43° [013], and 54.7° [001] polar angles from the normal to the surface, while the angular values of the chains direction in the (110) surface are 26° [130], 35° [111], 45° [100], and 60° [011]. Although the above sets of angular values for fcc and bcc Fe are rather close to each other, one must consider that the atomic distances along the atoms in the chains are rather different, i.e., 1.22, 0.71, 1.83, and 1.0 lattice parameter units in the fcc, while for the bcc surface the interatomic distances are 2.23, 0.86, 1.0, and 2.3. In fact, a longer atomic distance along the chains results in a reduced intensity of emission due to inelastic processes. As a consequence, the main intensities will be observed at 19.2° and 35° for the fcc while at 35° and 45° for the bcc. This implies that an appreciable modification of the KED patterns reported in Figs. 5(b) and (e) is observed, consisting in an apparent rotation of 30 degrees of the whole KED pattern, reflecting the modification of the experimental KED patterns as the Fe film thickness exceeds about 6 Å.

The fact that the early Fe layers are growing in a fcc crystalline structure (γ -Fe) and then relax in the standard bcc-Fe phase has been also confirmed by a previous x-ray diffraction analysis which yielded information on the interplanar distances orthogonal to the surface.³⁰ In fact, for small Fe layer thicknesses, the Fe interplanar distance coincides with that expected for bulk fcc-Cu (2.088 Å), which is very close to that extrapolated from bulk γ -Fe data 2.070 Å. As the Fe layer thickness increases above 8–10 Å, the interplanar distance decreases approaching the value expected for bcc-Fe (2.027 Å).

To summarize the results on the structural characterization of Cu/Fe/Cu/Si(111) heterostructures, we can assert that the growth of Fe on Cu(111) occurs first by formation of a few pseudomorphic layers and then by the growth of three-dimensional bcc Fe(110) domains in all the possible orientations compatible with the sixfold symmetry of the substrate. This is an example of the Stranki-Krastanov³¹ mode of growth, i.e., of pseudomorphic layers followed by the formation of domains rotationally related to the symmetry of the substrate. These results are in agreement with the experimental results obtained Tian *et al.*⁷ for Fe films deposited on a Cu single crystal as well as with the molecular dynamics theoretical results presented by Kadau *et al.*^{32,33}

IV. SMOKE RESULTS

A. Longitudinal geometry

Representative longitudinal hysteresis loops measured at room temperature for Fe films with thickness between 110 and 4 Å are shown in Fig. 6. For Fe films thicker than 6 Å, the loop remanence is relatively large, as characteristic of easy M - H loops, whereas the loops taken with the applied field normal to the film plane, which are not shown here, exhibit a linear behavior and an insignificant remanence. This indicates that the magnetization easy axis lies in the film plane, in agreement with the expected in-plane alignment of the magnetization at sufficiently large film thicknesses, due to the predominant contribution of the magnetostatic term in the magnetic free energy. For Fe films thinner than 6 Å, we did not detect any hysteresis loop both in the longitudinal and the polar geometry at room temperature because of the low value of the Curie temperature. However,

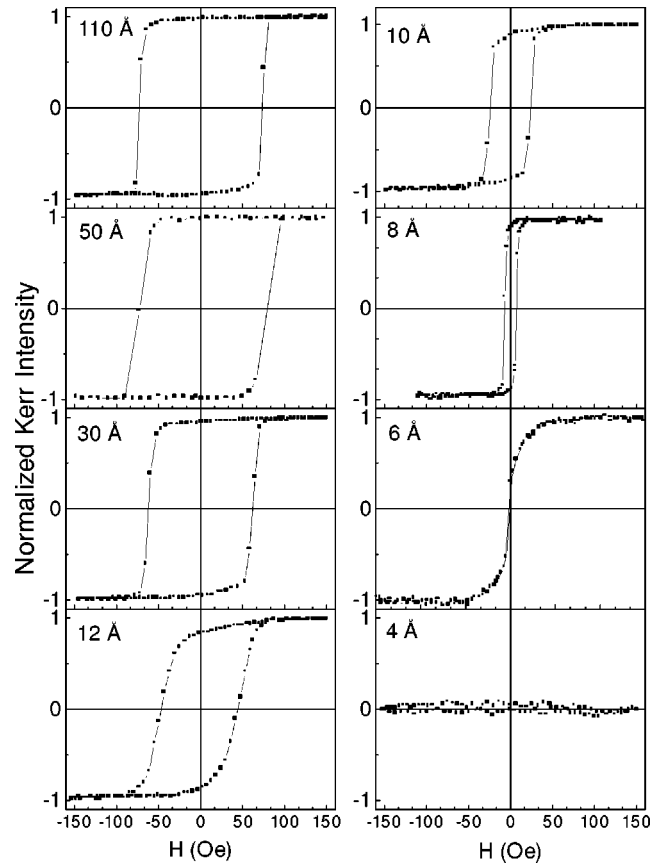


FIG. 6. Room temperature longitudinal SMOKE loops for Fe films whose thickness is reported in the figure. The external field intensity varies in the range $-150, +150$ Oe.

low temperature (<50 K) measurements show that these films are ferromagnetic with the magnetization orientation perpendicular to the film plane.³⁴

The analysis of the longitudinal Kerr intensity, reported in Fig. 7, revealed that two different ranges of Fe thickness can

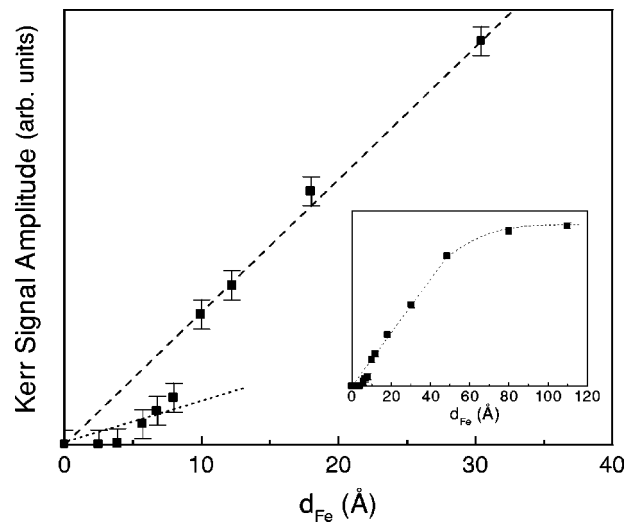


FIG. 7. Kerr signal amplitude in the longitudinal configuration as a function of Fe film thickness. It can be seen that two regimes of almost linear behavior can be identified, characterized by different slopes. The inset shows that for Fe thicknesses larger than 70 Å a saturation of the Kerr signal is observed because of the finite penetration depth of light.

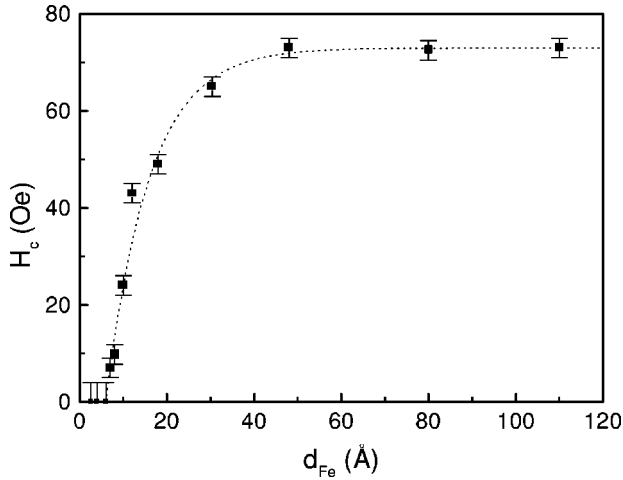


FIG. 8. Thickness dependence of the coercive field of the longitudinal M - H loops. The dotted curve is a guide to the eye.

be identified, lower and higher than approximately 10 Å, each of them characterized by a roughly linear behavior with different slopes. This change of slope happens in the same thickness range where the structural fcc-bcc transformation has been observed and can be interpreted as due to the presence of an fcc phase of iron with lower magnetic moment with respect to the bcc phase, i.e., by a different value of the saturation magnetization.^{9,35} This value can be estimated to be about three times smaller than that corresponding to the bcc Fe phase. If we assume the transformed bcc Fe films ($d_{\text{Fe}} > 10$ Å) to have a bulk moment of $2.2 \mu_B/\text{atom}$, the fcc Fe(111) films should have a moment close to that previously obtained by Gradmann *et al.*³ who found $0.6 \mu_B/\text{atom}$. The observed behavior also provides an experimental confirmation that the Kerr signal depends linearly on the thickness of the Fe layer as far as the film thickness is lower than the light penetration depth. A saturation effect is only observed for Fe thicknesses larger than 70 Å, in agreement with the observation made by Qiu *et al.*³⁶ in ultrathin Fe(110) films.

From a quantitative analysis of the SMOKE loops we also determined the behavior of the coercive field H_c which is plotted in Fig. 8 as a function of the Fe film thickness. H_c exhibits a sudden increase for thicknesses higher than 6 Å, i.e., simultaneously to the structural fcc to bcc transition, reaching a constant value of about 70 Oe for thicknesses above 50 Å. We have previously shown that this structural transformation is accompanied by the appearance of three-dimensional islands in the KS orientation upon the first pseudomorphic Fe layers. It is equally well known that islands formation and disorder in magnetic systems increase the coercive field.³⁷ These two arguments taken together allow us to interpret the rapid rise in the coercive field vs Fe film thickness as being due the increasing disorder associated with the islands growth and we can therefore take the onset of the rapid increase in H_c as an estimate of the critical thickness (≈ 6 Å) above which the fcc-bcc transition occurs.

B. Polar geometry

As a second step of our SMOKE characterization we performed high field polar loops to saturate the film along the normal to the surface and to determine the value of the out-

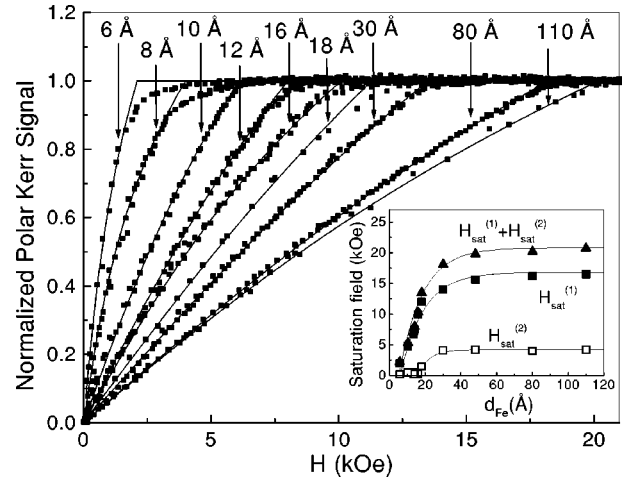


FIG. 9. Experimental magnetization data in the polar SMOKE configuration for Fe films with different thicknesses. The continuous curves are calculated by a best-fit procedure. The inset shows the behavior of the first-, second-order, and total saturation fields determined by a best-fit to the experimental polar loops for Fe films of different thicknesses.

of-plane anisotropy constants. The sequence of experimental SMOKE loops is presented in Fig. 9. From a direct observation of the loops one can see that the saturation field is lower than that expected from shape anisotropy alone assuming the bulk bcc value $4\pi M_s = 21$ kOe. This indicates a positive (i.e., out-of-plane) contribution from the uniaxial anisotropy. Concerning the loop shape, it appears a predominant linear approach to the saturation, due to the first-order anisotropy, followed by a slight curvature for high magnetic fields caused by the presence of a second-order anisotropy term. Therefore, the general expression for the magnetic free energy density can be written as³⁸

$$E = -K^{\text{eff}(1)} \cos^2 \theta - K^{\text{eff}(2)} \cos^4 \theta - M_s H \cos \theta, \quad (1)$$

where θ is the angle between the magnetization and the film normal, and $K^{\text{eff}(1)} \cos^2 \theta$ and $K^{\text{eff}(2)} \cos^4 \theta$ represent the first- and the second-order anisotropy energy terms, respectively. The last term describes the interaction between the external applied field and the magnetization. The equilibrium magnetization orientation as a function of the magnetic field strength is given by

$$\cos \theta_{eq} = \frac{H}{H_{\text{sat}}^{(1)} + H_{\text{sat}}^{(2)} \cos^2 \theta_{eq}}, \quad (2)$$

where $H_{\text{sat}}^{(1)} = -2K^{\text{eff}(1)}/M_s$ and $H_{\text{sat}}^{(2)} = -4K^{\text{eff}(2)}/M_s$ are the first- and second-order saturation fields, respectively. A quantitative determination of $H_{\text{sat}}^{(1)}$ and $H_{\text{sat}}^{(2)}$ has been obtained from a best fit of the experimental data to the calculated magnetization curves, showing that the main contribution to the magnetic energy comes from the first-order anisotropy, being the second-order anisotropy constants appreciably smaller, even if not negligible, as shown in the inset of Fig. 9. These results are in agreement with the previous investigation on Fe based multilayers.³⁹ In order to achieve a deeper insight into the physical meaning of the anisotropy constants, it is useful to subtract the shape anisot-

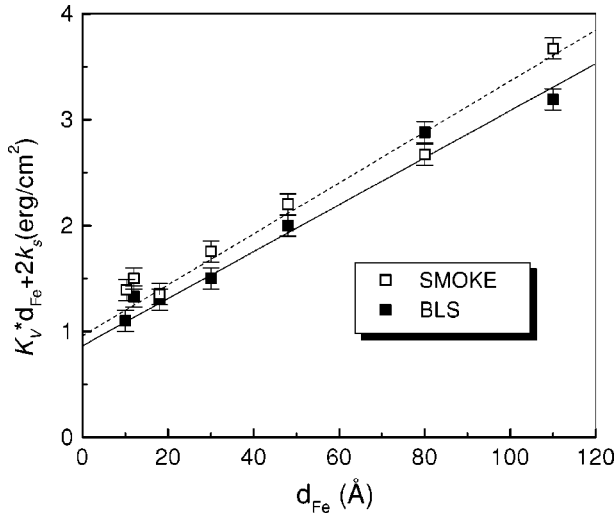


FIG. 10. Experimental values of the intrinsic uniaxial anisotropies determined by SMOKE (open squares) and BLS (full squares) vs the Fe layer thickness. The straight line is the result of a linear least-squares fit to the data based upon the model described in the text.

ropy energy from the first order anisotropy and distinguish between a bulk and an interface contribution. One therefore has

$$\begin{aligned} H_{\text{sat}}^{(1)} &= -\frac{2K^{\text{eff}(1)}}{M_s} = -\frac{2}{M_s} \left(-2\pi M_s^2 + K_V + 2\frac{k_s}{d} \right) \\ &= 4\pi M_s - \frac{2K_V}{M_s} - 4\frac{k_s}{dM_s}. \end{aligned} \quad (3)$$

In Fig. 10 the behavior of $K_V \cdot d + 2k_s$ is plotted as a function of d . A linear behavior is observed, and the intrinsic volume and interface anisotropy constants, K_V and k_s , correspond to the slope and the intercept of the linear regression curve, respectively. The positive sign of these anisotropy constants indicates that the intrinsic anisotropy favors the magnetization easy axis to be perpendicular to the film plane. In addition, the value K_V is rather different, five times greater than the magnetocrystalline volume anisotropy for bulk Fe,⁴⁰ indicating that some additional contributions such as, for example, magnetoelastic anisotropy, comes to play a significant role in determining the magnetic anisotropy.

V. BRILLOUIN LIGHT SCATTERING RESULTS AND DISCUSSION

Different from SMOKE, BLS is a dynamic technique, testing spin-wave excitations with wavelength comparable to that of light. The anisotropy contributions which are sources of additional effective fields in the ferromagnetic film, are felt by the precessing spins and can be derived from a measurement of the spin-wave frequency as a function of either the applied field or the film thickness. Figure 11 shows a sequence of experimental BLS spectra relative to films with different thicknesses, for an external field of 1 kOe. In addition to the dominating peak due to elastically scattered light, the peak due to Damon-Eshbach⁴¹ (DE) spin wave is clearly observed at frequencies in the range 3–21.5 GHz. This is the

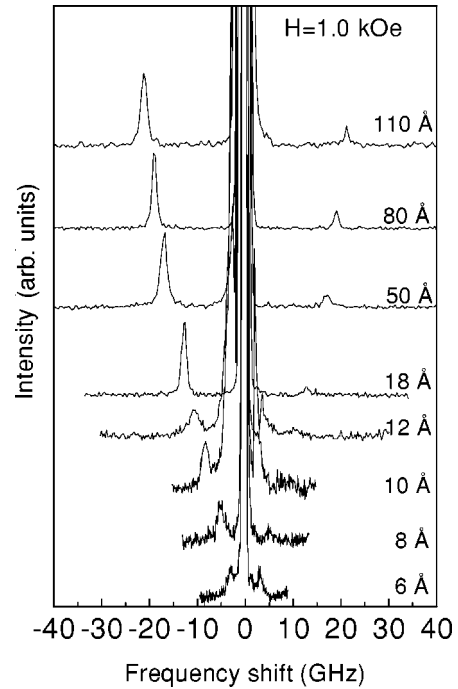


FIG. 11. Room temperature Brillouin spectra of epitaxial Cu/Fe/Cu/Si(111) heterostructures with different thicknesses of the Fe film for an external field of 1.0 kOe, applied in the film plane.

only peak present in our spectra, because the ratio between the film thickness and magnon wavelength is so low that bulk standing modes are at higher frequencies, not accessible in our experiments.⁴² The DE peaks exhibit a remarkable Stokes–anti-Stokes asymmetry, caused by the elliptical spin precession, typical of magnons in thin ferromagnetic films of absorptive materials.⁴³

We have carried out a study of the frequency dependence of the DE mode on the magnetic field strength for all the Cu/Fe/Cu/Si(111) heterostructures with Fe thickness larger than 6 Å, i.e., characterized by a practically constant value of the saturation magnetization. The experimental data relative to the frequency of the DE peak have been fitted to the curves calculated by using the following analytical expression:⁴⁴

$$\begin{aligned} \left(\frac{\omega}{\gamma} \right)^2 &= \left\{ \left[H + \frac{2A}{M_s} q_{\parallel}^2 - \frac{2}{M_s} \left(K_V + \frac{2k_s}{d} \right) \right. \right. \\ &\quad \left. \left. + 4\pi D M_s (1 - q_{\parallel} d / 2) \right] \right. \\ &\quad \left. \times \left(H + \frac{2A}{M_s} q_{\parallel}^2 + 2\pi D M_s q_{\parallel} d \right) \right\}, \end{aligned} \quad (4)$$

where $\gamma = \gamma_e g / 2$, with $\gamma_e = 1.759 \times 10^7$ Hz/Oe, is the gyromagnetic ratio, A is the exchange stiffness constant, and D is the demagnetizing factor which is $D = 1 - 0.2338/n$ with n the number of monolayers.⁴⁵ Both the experimental frequencies and the fitting curve are reported in Fig. 12. Qualitatively, the almost linear dependence of the spin-wave frequency on the applied field, with extrapolated positive intercept on the frequency axis, indicates that all these samples are in-plane magnetized, as already shown by

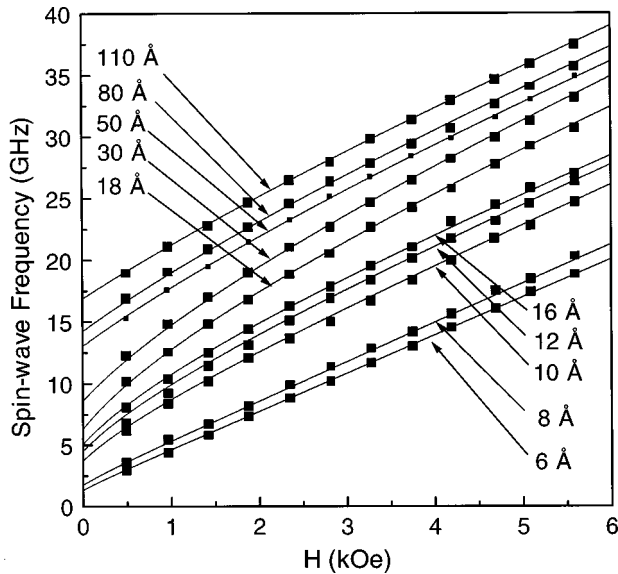


FIG. 12. Magnetic field dependence of the DE surface mode frequency for Cu/Fe/Cu/Si(111) heterostructures with Fe thickness in the range between 6 and 110 Å. Continuous curves are obtained by a best fit procedure using the analytical expression for the spin-wave frequency in the ultrathin film approximation.

SMOKE measurements.¹⁹ Quantitatively, from a best fit procedure of the calculated curves to the experimental points we determined for each specimen the value of the spectroscopic separation factor g and of the anisotropy constant $K_V/d + 2k_s$, taking the exchange constant and the saturation magnetization fixed at their values for bcc iron: $A = 2.0 \mu\text{erg/cm}$ and $4\pi M_s = 21.0 \text{ kOe}$. In such a way we obtained $g = 2.17 \pm 0.03$ which is in good agreement with that previously found in Fe films by BLS.⁴⁶ Concerning the anisotropy constants, the behavior of $K_V d + 2k_s$ as a function of d is plotted in Fig. 12 together with those previously determined by first-order SMOKE data (open squares). From a linear regression of the BLS data we obtained $K_V = (2.2 \pm 0.2) \times 10^6 \text{ erg/cm}^3$ and $k_s = (0.43 \pm 0.02) \text{ erg/cm}^2$ which compare very well with the first order SMOKE results [$K_V = (2.4 \pm 0.1) \times 10^6 \text{ erg/cm}^3$ and $k_s = (0.48 \pm 0.03) \text{ erg/cm}^2$]. Both BLS and SMOKE yield a positive sign of the intrinsic anisotropy, indicating that the surface normal is a magnetic easy axis for this anisotropy contribution. FMR measurements previously performed by Heinrich *et al.*⁴⁷ on epitaxial Cu/Fe(001) Au trilayers, gave the same sign for the interface anisotropy constant, but larger magnitude (0.62 erg/cm^2), owing presumably to the different crystallographic orientation and to the exposure of one Fe surface to Au rather than both to Cu.

In order to better clarify the role of interface anisotropy, we plot in Fig. 13 the behavior of the DE mode frequency as a function of the Fe film thickness, for a constant value of the applied magnetic field of 1.0 kOe. It can be seen that the agreement between the experimental data and the theoretical curve, calculated with the parameters obtained from the fitting procedure described above, is quite satisfactory. In particular, the frequency reduction observed below 30 Å is due to the influence of the out-of-plane interface anisotropy constant k_s . In this range of thicknesses the Damon-Eshbach surface mode becomes an interface-anisotropy-dominated

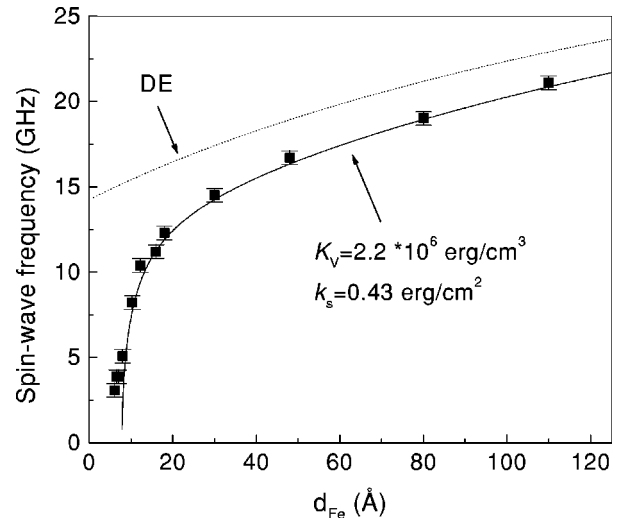


FIG. 13. Frequency dispersion of the Damon-Eshbach surface mode vs Fe film thickness for an applied field of 1 kOe. The continuous line is a fit to the experimental data, while the dotted line is the behavior expected for the DE mode without considering exchange interaction and interface anisotropy.

mode, as expected from the $1/d$ dependence of the interface anisotropy contribution.⁴⁸ For the sake of comparison, we have also reported in the same figure the behavior of the DE mode calculated in absence of any interface anisotropy (dotted curve). Finally, we stress that for Fe thicknesses lower than 10 Å a slight discrepancy between the spin-wave frequency and the calculated curve is observed. This deviation, which occurs just in the region where the structural transformation of iron takes place, can be attributed to the reduced magnetic moment of the fcc phase of iron already put in evidence by SMOKE measurements and not taken into account in our calculation.

CONCLUSIONS

Epitaxial Cu/Fe/Cu heterostructures with Fe film thicknesses between 2.5 and 110 Å were successfully grown on 7×7 -Si(111) substrates, using metal-metal epitaxy on silicon. A detailed LEED and KED investigation showed that the growth of Fe on Cu(111) occurs first by formation of pseudomorphic Fe layers and then, for coverage higher than 6–8 Å, by growth of three-dimensional bcc Fe(110) domains in the Kurdjumov-Sachs orientation. SMOKE analysis performed at room temperature revealed that Fe films thicker than 5 Å are in-plane magnetized. In addition, the Kerr signal increases and two different ranges of thicknesses can be identified, each of them characterized by a different value of the saturation magnetization. This change happens just in the same thickness range where the structural fcc-bcc transformation has been observed, suggesting that fcc pseudomorphic Fe layers are characterized by a low-spin ferromagnetic phase. A sudden increase of the coercive field relative to the longitudinal loops was also observed with increasing Fe thickness above 8 Å, because of the growth of bcc(110) islands which introduce structural disorder in the magnetic film. High field polar SMOKE loops enabled us to determine the first- and second-order out-of-plane anisotropy fields. In order to quantitatively compare these results with those of a

dynamic technique, the anisotropy constants were also measured by BLS, studying the spin wave frequency dependence on the applied magnetic field. We found an excellent agreement, in both sign and magnitude, between the BLS data and the first-order anisotropy constants measured by SMOKE. This validates the assumption that in a BLS experiment the magnetization is merely perturbed through small angles about its equilibrium direction and therefore only first-order anisotropy energy is probed by this dynamic technique. Both BLS and SMOKE yield a positive sign of the intrinsic anisotropy, indicating that the surface normal is a magnetic easy axis for this anisotropy contribution, even if, owing to the dominating shape anisotropy, the magnetization lies in

the film plane at room temperature. The influence of the out-of-plane interface anisotropy was also put in evidence by Brillouin scattering measurements which accounted for a marked frequency decrease of the Damon-Eshbach mode for Fe thicknesses below 30 Å.

ACKNOWLEDGMENTS

We would like to thank R. Bernardini and S. Fusari for sample preparation and the structural characterization. This work was supported by INFM under the SIMBRIS advanced research project and by CNR.

*Author to whom correspondence should be addressed. Fax: +39 075 44666. Electronic address: gubbiotti@pg.infn.it

- ¹V. L. Moruzzi, P. M. Marcus, and J. Kübler, *Phys. Rev. B* **39**, 6957 (1989), and references therein.
- ²J. G. Wright, *Philos. Mag.* **24**, 217 (1971).
- ³U. Gradmann, W. Kummerle, and P. Williams, *Thin Solid Films* **34**, 249 (1976).
- ⁴R. Halbauer and U. Gonser, *J. Magn. Magn. Mater.* **35**, 55 (1978).
- ⁵D. Pescia, M. Stapanoni, G. L. Bona, A. Vaterlaus, R. F. Willis, and F. Meier, *Phys. Rev. Lett.* **58**, 2126 (1987); W. A. A. Macedo and W. Kuene, *ibid.* **61**, 475 (1988); J. Thomassen, F. May, B. Feldmann, M. Wutting, and H. Ibach, *ibid.* **69**, 3831 (1992); R. D. Ellerbrock, A. Fuest, A. Schatz, W. Kuene, and R. A. Brand, *ibid.* **74**, 3053 (1995); S. Muller, P. Bayer, C. Reischl, K. Heinz, B. Feldmann, H. Zillgen, and M. Wuttig, *ibid.* **74**, 765 (1995); J. Giergiel, J. Shen, J. Woltersdorf, A. Kirilyuk, and J. Kirschner, *Phys. Rev. B* **52**, 8528 (1995), and references therein.
- ⁶W. Kummerle and U. Gradmann, *Phys. Status Solidi* **45**, 171 (1978).
- ⁷D. Tian, F. Jona, and P. M. Marcus, *Phys. Rev. B* **45**, 11 216 (1992).
- ⁸W. Kummerle and U. Gradmann, *Solid State Commun.* **24**, 33 (1977); Y. Darici, J. Marcano, H. Min, and P. A. Montano, *Surf. Sci.* **185**, 566 (1988); M. T. Kief and W. F. Egelhoff, Jr., *J. Vac. Sci. Technol. A* **11**, 1661 (1993).
- ⁹J. Shen, M. Klaua, P. Ohresser, H. Jenniches, J. Barthel, Ch. V. Mohan, and J. Kirschner, *Phys. Rev. B* **56**, 11 134 (1997).
- ¹⁰B. Hillebrands, in *Light Scattering in Solids VII*, edited by M. Cardona and G. Güntherodt, Springer Series in Topics in Applied Physics (Springer-Verlag, Berlin, in press), and references therein.
- ¹¹M. De Crescenzi, R. Gunnella, R. Bernardini, M. De Marco, and I. Davoli, *Phys. Rev. B* **52**, 1806 (1995).
- ¹²M. Erbudak, M. Hochstrasser, and E. Wetli, *Mod. Phys. Lett. B* **8**, 1759 (1994).
- ¹³J. R. Sandercock, in *Light Scattering in Solids III*, edited by M. Cardona and G. Güntherodt, Vol. 51 of Springer Series in Topics in Applied Physics (Springer-Verlag, Berlin, 1982), p. 173.
- ¹⁴G. Gubbiotti, G. Carlotti, and G. Socino, in *Nanophase Materials*, edited by E. Bonetti and D. Fiorani (Trans Tech, Zurich, 1995), p. 215.
- ¹⁵L. Albin, Tesi di Laurea, University of Perugia, 1998.
- ¹⁶C. A. Ballentine, R. L. Fink, J. Araya-Pochet, and J. L. Erskine, *Appl. Phys. A: Solids Surf.* **49**, 459 (1989).
- ¹⁷R. M. A. Azzam and N. M. Bashara, in *Ellipsometry and Polar-*

ized Light (North-Holland, Amsterdam, 1977).

- ¹⁸G. Gubbiotti, L. Albin, G. Carlotti, G. Socino, S. Fusari, and M. De Crescenzi, *Surf. Sci.* **433-435**, 685 (1999).
- ¹⁹G. Gubbiotti, G. Carlotti, G. Socino, F. D'Orazio, F. Lucari, R. Bernardini, and M. De Crescenzi, *Phys. Rev. B* **56**, 11 073 (1997).
- ²⁰G. Gubbiotti, G. Carlotti, S. Loreti, C. Minarini, R. Gunnella, and M. De Crescenzi (unpublished).
- ²¹St. Tosch and H. Neddermeyer, *Surf. Sci.* **211/212**, 133 (1989).
- ²²A. T. Gorton, G. Bitsianes, and T. L. Joseph, *Trans. Metall. Soc. AIME* **233**, 1519 (1965).
- ²³D. Tian, H. Li, F. Jona, and P. M. Marcus, *Solid State Commun.* **80**, 783 (1991).
- ²⁴A. Zangwill, *Physics at Surfaces* (Cambridge University Press, Cambridge, 1988), p. 422.
- ²⁵R. Ramirez, A. Rahman, and I. K. Schuller, *Phys. Rev. B* **30**, 6208 (1984).
- ²⁶A. Kobayashi and S. Das Sarma, *Phys. Rev. B* **35**, 8042 (1987).
- ²⁷E. Bauer and Jan H. van der Merwe, *Phys. Rev. B* **33**, 3657 (1986).
- ²⁸J. Mustre de Leon, J. J. Rehr, C. R. Natoli, C. S. Fadley, and J. Osterwalder, *Phys. Rev. B* **39**, 5632 (1989).
- ²⁹M. P. Seah and W. A. Dench, *Surf. Interface Anal.* **1**, 2 (1979).
- ³⁰G. Gubbiotti, L. Albin, G. Carlotti, S. Loreti, C. Minarini, and M. De Crescenzi, *Surf. Sci.* **433-435**, 680 (1999).
- ³¹A. Zangwill, *Physics at Surfaces* (Ref. 24).
- ³²K. Kadau, R. Meyer, and P. Entel, *Surf. Rev. Lett.* **6**, 35 (1998).
- ³³K. Kadau, R. Meyer, and P. Entel, *J. Magn. Magn. Mater.* **198-199**, 531 (1999).
- ³⁴G. Gubbiotti, G. Carlotti, F. D'Orazio, F. Lucari, R. Gunnella, and M. De Crescenzi, *Surf. Sci.* (to be published).
- ³⁵J. Zak, E. R. Moog, C. Liu, and S. D. Bader, *J. Magn. Magn. Mater.* **89**, 107 (1990).
- ³⁶Z. Q. Qiu, J. Pearson, and S. D. Bader, *Phys. Rev. B* **45**, 7211 (1992).
- ³⁷A. Paoluzi, in *Magnetic Properties of Matter*, edited by F. Borsa and V. Tognetti (World Scientific, Singapore, 1988), p. 56.
- ³⁸M. J. Pechan and I. K. Schuller, *Phys. Rev. Lett.* **59**, 132 (1987).
- ³⁹M. J. Pechan, E. E. Fullerton, W. Robertson, and M. Grimsditch, *Phys. Rev. B* **52**, 3045 (1995).
- ⁴⁰E. P. Wohlfarth, in *Ferromagnetic Materials*, edited by E. P. Wohlfarth (North-Holland, Amsterdam, 1980), p. 39.
- ⁴¹R. W. Damon and J. R. Eshbach, *J. Phys. Chem. Solids* **19**, 308 (1961).
- ⁴²G. Gubbiotti, G. Carlotti, and B. Hillebrands, *J. Phys. C* **10**, 2171 (1998).

- ⁴³R. E. Camley, P. Grünberg, and C. M. Mayr, Phys. Rev. B **26**, 2609 (1982).
- ⁴⁴This formula is derived from R. L. Stamps and B. Hillebrands, Phys. Rev. B **44**, 12 417 (1991), assuming a uniaxial magnetic energy of the form $E = -(K_V + 2k_s/d)\cos^2 \theta$.
- ⁴⁵B. Heinrich, S. T. Purcell, J. R. Dutcher, K. B. Urquhart, J. F. Cochran, and A. S. Arrott, Phys. Rev. B **38**, 12 879 (1988).
- ⁴⁶P. Grünberg, in *Light Scattering in Solids V*, edited by M. Cardona and G. Güntherodt, Springer Series in Topics in Applied Physics (Springer-Verlag, Berlin, 1989), and references therein.
- ⁴⁷B. Heinrich, Z. Celinski, J. F. Cochran, A. S. Arrott, and K. Myrtle, J. Appl. Phys. **70**, 5769 (1991).
- ⁴⁸G. Carlotti and G. Gubbiotti (unpublished).